Oxidation of Organic Films by Beams of Hydroxyl Radicals†

Timothy M. D'Andrea,[‡] Xu Zhang,[‡,§] Evan B. Jochnowitz,[‡,||] T. G. Lindeman,[⊥] C. J. S. M. Simpson,[#] Donald E. David,[‡,+] Thomas J. Curtiss,[£] John R. Morris,[△] and G. Barney Ellison*[,‡]

Department of Chemistry & Biochemistry, University of Colorado, Boulder, Colorado 80309-0215, Jet Propulsion Laboratory, California Institute of Technology, 4800 Oak Grove Drive, Pasadena, California 91109-8099, Institute for Physical Chemistry, University of Basel, Klingelbergstrasse 19, CH-4056 Basel, Switzerland, Department of Chemistry, Colorado College, Colorado Springs, Colorado 80903-3298, Physical Chemistry Laboratory, Oxford University, South Parks Road, Oxford, OX1 3QZ, United Kingdom, Department of Chemistry & Biochemistry, Integrated Instrument Design Facility, CIRES, University of Colorado, Boulder, Colorado 80309-0216, The Aerospace Corporation, P.O. Box 92957, Mail Station M2/341, Los Angeles, California 90009-2957, and Chemistry Department, Virginia Tech, 107 Davidson Hall, Blacksburg, Virginia 24061-0001

Received: October 1, 2007; In Final Form: November 16, 2007

We have studied the oxidation of self-assembled monolayers (SAMs) of alkanes and alkenes with a thermal beam of OH radicals. The target films were produced by bonding alkane thiols and alkene thiols to a gold surface and the SAMs are mounted in a vacuum chamber at a base pressure of 10^{-9} Torr. Hydroxyl radicals were produced by a corona discharge in an Ar/H_2O_2/water mixture. The resultant molecular beam was scanned by an electrostatic hexapole and the OH radicals [$4 (\pm 1) \times 10^{11}$ OH radicals cm^{-2} sec^{-1}] were focused onto the target SAM. All of the hydroxyl radicals impinging on the SAM surface are rotationally ($J'' \leq 5/2$) cold. The vibrational temperature of the radicals is estimated to be 1700−3400 K which implies that between 5% and 22% of the hydroxyl radical beam is $OH_{v=1}$ and the remainder (95% to 78%) is $OH_{v=1}$. The collision energy of the beam with the SAM is 333 cm^{-1} corresponding to a 485 K thermal beam. We employed reflection/absorption infrared spectroscopy (RAIRS) to monitor the reactivity of OH with an alkane and an alkene SAM. RAIRS demonstrated that a 10 min dose of OH radicals largely destroys the CH_3- groups at the interface. This corresponds to a deposition of 2.4×10^{14} OH cm^{-2} or about 60% of the SAM monolayer. Oxidation of an undec-10-ene-1-thiol ($HS(CH_2)_9HC{=}CH_2$) SAM with OH radicals proceeded more quickly with all the terminal alkenes, $-CH{=}CH_2$, eliminated within 5 min following deposition of 1.2×10^{14} radicals. We believe that the OH radicals initiate a radical-induced polymerization of the alkene film.

Introduction

Reactions of radicals with hydrocarbon films are important examples of heterogeneous chemistry. We have designed and built an apparatus that enables self-assembled monolayers (SAMs) to be dosed with a calibrated beam of hydroxyl radicals. The subsequent oxidation of the hydrocarbon film is monitored by infrared spectroscopy. With this new apparatus, we have observed that alkane and alkene SAMs are attacked at close to the collision frequency by OH at room temperature.

The homogeneous, gas-phase reactions of OH radicals with all volatile organic compounds (VOCs) are of great importance in atmospheric chemistry.[1−7] All clouds and ice particles nucleate on micrometer sized atmospheric particles called aerosols.[8] We believe that the heterogeneous chemistry of organic aerosols is important in their evolution as they rise in the atmosphere. In 1999, a model[9] was proposed for marine aerosols that described them as inverted micelles. This model described a chemical structure for aerosols, accounted for their organic content, and predicted the chemical evolution or atmospheric processing of the organic material. Hydrophobic surfactants are carried up from the surface of the ocean and born into the atmosphere on the surface of saline water droplets. Figure 1 depicts reactions of these micrometer sized water droplets coated with a film of surfactants. The organic surfactants are predicted to be bound to the saline aqueous drop by several polar groups such as $-N(CH_3)_3^+$, $-CO_2^-$, and so forth. These polar functional groups are embedded in the water droplet and are indicated by the dot, (○). The inverted micelle model predicts[9] that the organic surfactants of the aerosol would be steadily oxidized in the atmosphere. On the basis of the density[3,5,10] of OH radicals, $\rho(OH) = 10^6$ cm^{-3}, it was conjectured that the processing time would be 3−8 h. This processing by atmospheric radical chemistry transforms the organic film into a hydrophilic layer. Consequently, the oxidized aerosols are much better cloud condensation nuclei (CCN) than the nascent particles. As the surfactants are oxidized by atmospheric oxidants such as OH, O_3, O_2, or NO_3, the hydrophobic alkyl groups are transformed into alcohols, aldehydes, carboxylic acids, and so forth. Surfaces sprinkled with

† Part of the "James T. (Casey) Hynes Festschrift".
* Corresponding author. E-mail: barney@jila.colorado.edu.
‡ Department of Chemistry and Biochemistry, University of Colorado.
§ California Institute of Technology.
|| University of Basel.
⊥ Colorado College.
Oxford University.
+ CIRES, University of Colorado.
£ The Aerospace Corporation.
△ Virginia Tech.

10.1021/jp7096108 CCC: $40.75
Published on Web 12/19/2007

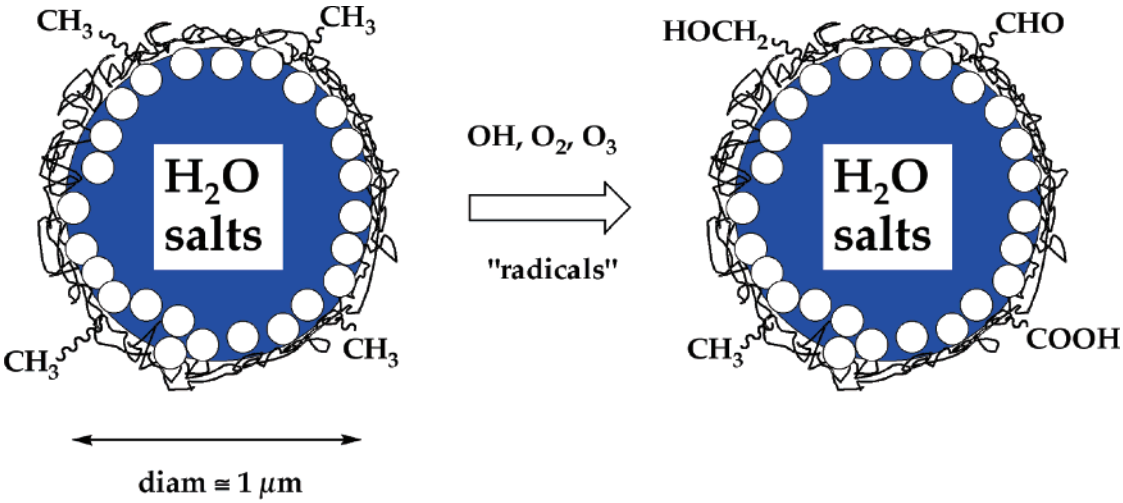

Figure 1. Micron-sized water droplets coated with a film of surfactants react with radicals and ozone. The organic surfactants are predicted to be bound to the saline aqueous drop by several polar groups such as $-N(CH_3)_3^+$, $-CO_2^-$, etc. These polar functional groups are embedded in the water droplet and are indicated by the dot, (○).

polar groups are easy[11] to "wet" and will be excellent CCN. Numerous laboratory reports[12−14] and recent field measurements[15] are consistent with several predictions[9] of the inverted micelle model.

The essence of the atmospheric processing described in Figure 1 is the heterogeneous oxidation of the organic film coating the water droplet. Since the hydroxyl radical is one of the most important atmospheric oxidants, we wish to understand the individual reaction steps that describe OH reacting with hydrocarbon films. Because of the large bond energy[16,17] of water [DH_{298}(H−OH) = 118.82 ± 0.07 kcal mol^{-1}] OH radicals will abstract H atoms when they strike a film of saturated organic molecules. The CH bond energies[18,19] of all alkanes are ≤100 kcal mol^{-1}, so this abstraction is exothermic by almost 1 eV.

The homogeneous reaction of hydroxyl radicals with alkanes in the gas phase has been extensively studied.[20] But the heterogeneous chemistry at a droplet/atmosphere interface might be different. It was[9] conjectured that OH would react at a nearly encounter-controlled rate with coated organic aerosols. There is now direct experimental evidence for the high rate of reactivity of OH with hydrocarbon films. For heterogeneous reactions, Bertram et al.[21] have measured OH loss via chemical ionization mass spectrometry in a flow tube reactor coated with organic species. Heterogeneous loss of OH was found to be very efficient; the reaction probability of OH radical with the organic film was estimated to be roughly 50%.

In order to understand the elementary steps of the heterogeneous oxidation chemistry in Figure 1, we dosed well-defined hydrocarbon films with OH radical beams under conditions where we could monitor the interfacial region by infrared (IR) absorption spectroscopy. We chose to mount hydrocarbon films as organic thiolate/gold SAMs because these samples[22] have well-characterized, dense, stable structures. Alkanethiols, RSH, spontaneously bind to Au to form gold alkanethiolates or RS^-Au^+. The binding energy, DH_{298}(RS−Au), has been reported[22] to be roughly 40 kcal mol^{-1}. Reflection/absorption infrared spectroscopy (RAIRS) is an exquisitely sensitive technique to monitor the chemical nature of the SAM by following changes in specific functional groups in the presence of many different groups.

Experimental Methods

We have undertaken a study of the reaction chemistry of OH radicals with hydrocarbon films by using self-assembled monolayers. A schematic diagram of the experimental apparatus is shown in Figures 2 and 3. The goal for this instrument is to produce intense beams of OH radicals and observe reactive scattering at the SAM. A FTIR spectrometer is used to monitor the oxidation state of the surface organic radicals.

The key component of the device in Figures 2 and 3 is an electrostatic hexapole apparatus[23−25] that separates OH radicals from other species present and focuses them into an intense beam. Symmetric-top molecules with a dipole moment, μ_D, (e.g., CH_3Cl) experience a harmonic radial force in the inhomogeneous electrostatic field produced with an ideal electrostatic hexapole because of their first-order Stark effect.[26] Consider an electric hexapole field produced by a set of six rods maintained at alternating, fixed potentials of $\pm V_0$ on an inscribed circle of radius r_0. The force exerted by a hexapole field is only in the plane perpendicular to the poles. The radial, harmonic force experienced[25] by a polar molecule in an ideal hexapole can be expressed in polar coordinates (r, ϕ) as:

$$F_r = -\frac{\partial E^{(1)}}{\partial \epsilon}\frac{\partial \epsilon}{\partial r} = \frac{\mu_D KM}{J(J+1)}\left(\frac{6V_0}{{r_0}^3}\right) r = -kr \qquad (1)$$

where $E^{(1)}$ is the first-order Stark energy, ϵ is the electric field strength, k is a force constant for radial motion, and J, K, M are the rotational quantum numbers of the molecule in state $|JKM\rangle$. When a beam of molecules diverging from a supersonic expansion enters the hexapole field with axial velocity v, the molecules will follow a sinusoidal path. For a single-loop trajectory where l is the effective length of the hexapole and m is the molecular mass, the focusing condition can be written as:

$$V_0 = \frac{\pi^2 {r_0}^3 m v^2}{6\, l^2 \mu_D}\left[\frac{-KM}{J(J+1)}\right]^{-1} \qquad (2)$$

In principle, by tuning V_0 to the appropriate voltage, one can focus a specific molecule in a single rotational state through the hexapole exit aperture.

Open-shell diatomic molecules in a $^2\Pi$ electronic state (e.g., OH, NO) have nearly degenerate pairs of states (Λ doublets) that exhibit nearly first-order Stark behavior at high electric field strengths.[23] Such diatomics with large dipole moments, for example, OH with its dipole moment[27,28] of 1.65520 ± 0.00010

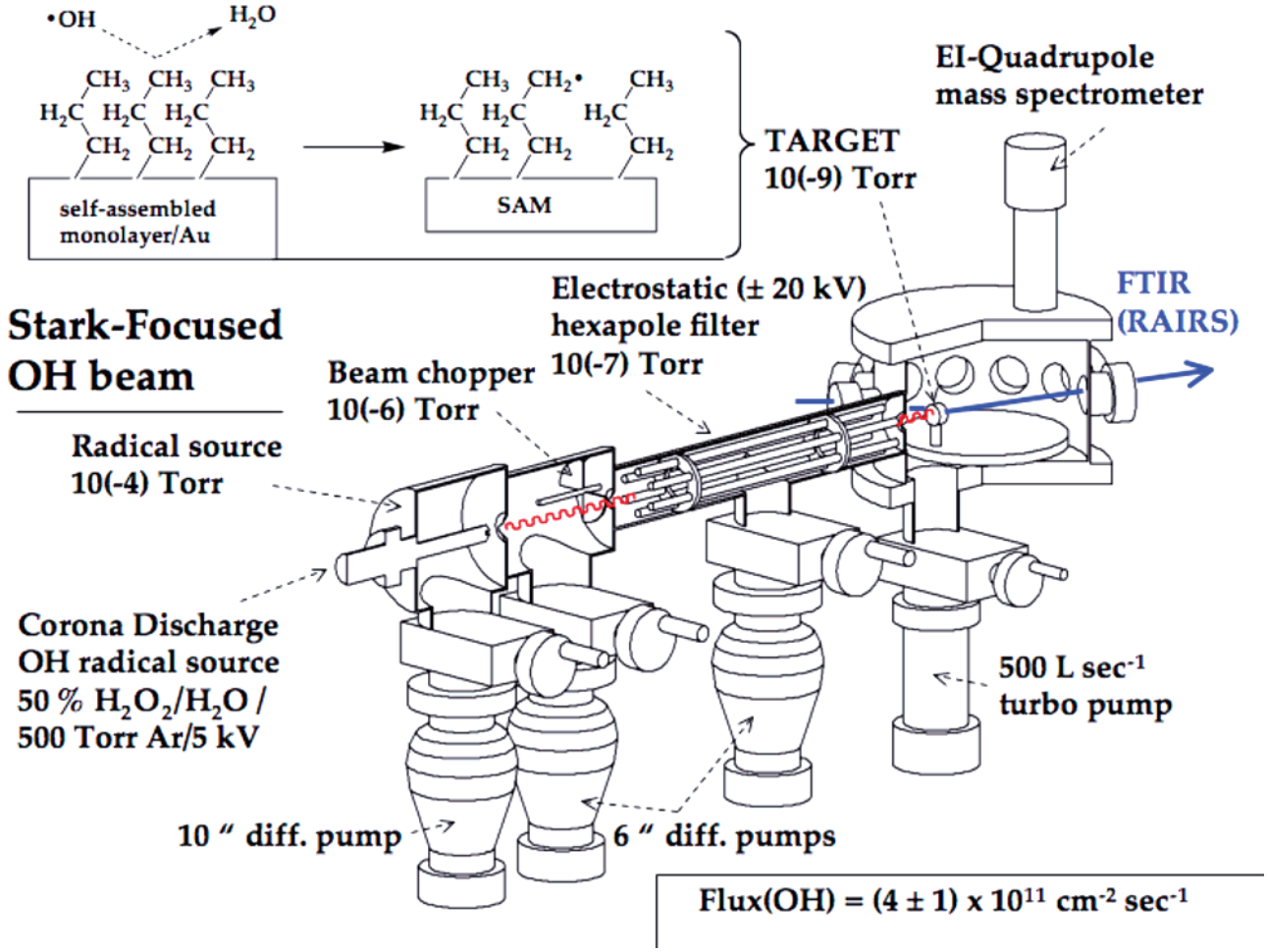

Figure 2. Overview of the OH/surface experimental apparatus. The goal for this instrument is to produce intense beams of OH radicals and observe reactive scattering at the SAM. A FTIR spectrometer is used to monitor the oxidation state of the surface organic radicals.

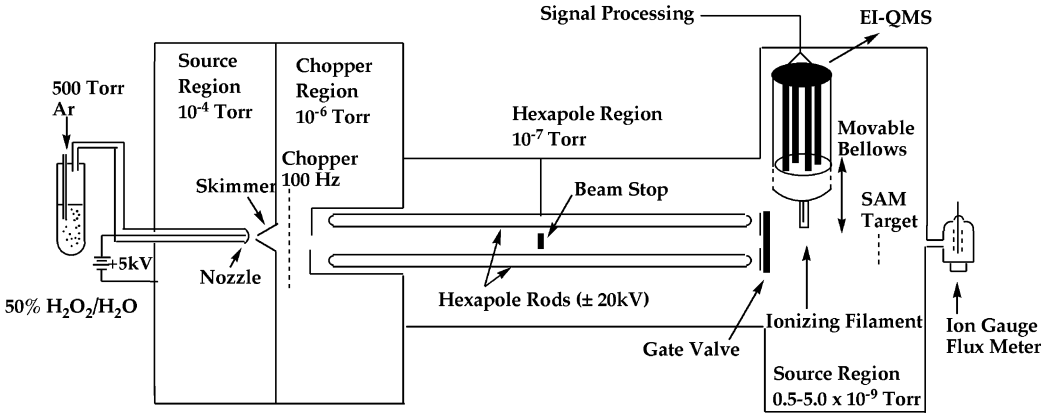

Dist. from nozzle aperture	Distance/cm	Radius/mm
Nozzle (aperture)	0	0.05
Skimmer (aperture)	1.0	0.75
Hexapole entrance collimator	8.5	1.8
Beam stop	62	1.3
Hexpole exit collimator	116	1.6
EI-QMS	120.2	-
SAM target	134.2	5.0
Ion gauge	140	2.5

Figure 3. Schematic diagram of the OH/surface experiment. The table contains some of the important dimensions of this apparatus.

D, can be selectively focused in a hexapole. Asymmetric tops generally exhibit weaker, nonlinear Stark behavior but can also be focused by inhomogeneous fields, generally at much higher field strengths than either symmetric tops or $^2\Pi$ diatomics.[23] Atoms will not be focused because they possess no electric dipole moment. Consequently, under appropriate conditions, the selectivity of hexapole focusing for OH can be exploited to purify a beam mixture.

Beams of OH Radicals. The apparatus shown in Figures 2 and 3 is patterned after the hydroxyl radical source pioneered by Curtiss et al.[25,29,30] One of the aims of the instrument is to produce intense, clean hydroxyl radical beams and to deliver them to the SAM target in a scattering chamber pumped to 10^{-9} Torr. A corona discharge[31,32] is an attractive radical source because it only produces H (^{2}S) atoms, O (^3P_J) atoms, and OH ($^2\Pi_{3/2}$) radicals from a rare gas/water source. If hydrogen peroxide is added to the source, fragmentation of HOOH will produce hydroxyl radicals: H_2O_2 + discharge → 2OH. Simulations confirm our empirical observation that the asymmetric tops H_2O and H_2O_2 cannot be focused at the operating voltages of our hexapole. It has also been found that, while hard expansions containing water vapor do produce asymmetric top water dimers $(H_2O)_2$ that can be readily focused, experiments show that such dimers do not survive the corona discharge environment.

The radical source in Figures 2 and 3 produces OH radicals by bubbling 500 Torr of Ar through a 50% solution of hydrogen peroxide in water and sending it through a corona discharge. The corona discharge consists of a 30 gauge Pt needle (roughly 250 μm diameter) which is surrounded by a quartz nozzle with a 0.1 mm diameter exit aperture. The Pt needle is biased at +5 kV relative to a grounded skimmer, as shown in Figure 3. The gases undergo a mild supersonic expansion from the nozzle then pass through a 1.5 mm diameter skimmer into the chopper chamber. The beam is modulated at 100 Hz with a 50% on−off pattern to allow for phase sensitive detection downstream with a commercial electron-impact quadrupole mass spectrometer, EI-QMS (Stanford Research Systems model 200 residual gas analyzer operated with an ionization energy of 70 eV). Once chopped, the molecular beam travels through a 3.6 mm diameter collimator and enters the differentially pumped electrostatic hexapole region, which is located 85 mm from the end of the nozzle. The hexapole region consists of 6 cylindrical stainless steel rods that are 1.067 m long and have an inscribed radius of 11.25 mm. In order to select and focus the OH radicals, we apply up to ±20 kV to the rods, which induces the OH radicals to travel in a nearly sinusoidal path around a 2.6 mm diameter stainless steel beam stop located directly in the middle of the hexapole rods.

The OH molecular beam exits the hexapole region through a 3.2 mm diameter collimator and enters the surface chamber where the EI-QMS can be used to measure the gas composition and flux of the beam. The EI-QMS is mounted in a linear vacuum feedthrough (1.202 m downstream of source nozzle) so that it can be moved into or out of the path of the beam. The analogue output of the EI-QMS is sent to the input of a lock-in amplifier (Ithaco Dynatrac model 391A), which uses the chopper frequency as the reference for phase sensitive detection in order to discriminate between species in the molecular beam and the background gases in the chamber. The flux of the beam is monitored by an on-axis ion gauge (Kurt J. Lesker Co. model G100F) located behind a 5 mm diameter aperture. A moveable 1 cm^2 self-assembled monolayer sample target can be inserted between the EI-QMS and the ion gauge to intercept the OH radicals.

Nearly all of the nonfocused molecules are blocked by the beam stop or by the chamber walls. A corona discharge of H_2O and H_2O_2 in Ar produces a mixture of OH, H, O, hydrogen peroxide, and water. The target hydroxyl radicals are in their ground state, OH X $^2\Pi_\Omega$, and are focused by the hexapole filter. Consequently, only OH radicals with $\mu_D(OH) = 1.6552$ D will be actively passed by the hexapole filter while the unwanted H_2O_2/H_2O molecules and the H and O atoms will be blocked by the beam stop and pumped away. The preferential focusing of OH was verified by mass spectrometry. We used the EI-QMS to monitor the signals for OH^+ (from hydroxyl radical), H_2O^+ (from water), and $H_2O_2^+$ (from hydrogen peroxide). The EI mass spectrum has been reported for hydroxyl radical,[33] water,[33] and hydrogen peroxide.[34] As expected, the dominant ions in the 70 eV EI mass spectrum of hydroxyl radical are OH^+, *m*/*z* 17, while for water it is H_2O^+, *m*/*z* 18. For hydrogen peroxide,[34] there is little fragmentation following 70 eV EI, and the $H_2O_2^+$ parent peak, *m*/*z* 34, is 5 times more intense[34] than the OH^+ fragmentation ion. During the operation of the OH radical source with the hexapole filter on and the beam stop in place, fluxes of up to $(3 \pm 1) \times 10^{10}$ H_2O molecules cm^{-2} s^{-1} have been observed by the EI-QMS but there is no measurable signal for $H_2O_2^+$ or for HOO^+. Consequently, we believe that no H_2O_2 survives to enter the target chamber (Figure 2).

How many hydroxyl radicals does the corona discharge make, and what is the translational energy of the beam? The beam exiting the corona discharge source contains a stream of OH radicals entrained in Ar atoms moving at a terminal[26,35] beam velocity, V_∞. If the ratio of heat capacities (C_p/C_v) is written as γ, this velocity is

$$V_\infty = \sqrt{\frac{2RT\gamma}{M(\gamma - 1)}} \tag{3}$$

For an atom like Ar, γ is 5/3 and V_∞(Ar beam) is calculated to be 5.6×10^4 cm s^{-1} at room temperature, 300 K. The velocity of Ar atoms emerging from this source with the corona discharge off has been measured[24] in an earlier paper to be $V(Ar) = 5.7 \times 10^4$ cm s^{-1}. When the corona discharge is operating, the $V_{discharge}(Ar)$ was observed[24] to be 6.85×10^4 cm s^{-1}. To be sure, the measured velocities were dependent on discharge conditions but without time-of-flight (TOF) measurements; this is the best estimate.

On the basis of our prior experience with measured beam velocities and rotationally resolved focusing spectra, a 500 Torr Ar/OH expansion behind a 0.1 mm diameter nozzle would be expected to produce a sharply peaked beam of OH radicals with rotational temperatures populating the few lowest rotational states (e.g., $J = 5/2$ and less). The discharge heats the nozzle somewhat, typically producing Ar seeded beam velocities on the order of 600−800 m/s. As a figure of merit, we have chosen (Hain, T. D.; Weibel, M. A.; Backstrand, K. M.; Curtiss, T. J. *J. Phys. Chem. A* **1997**, *101*, 7674) a value of 685 m/s for subsequent calculations on the basis of prior measured values. A sharply peaked, $\Delta T = 10$ K, 685 m sec^{-1} OH beam will have a translational energy of 41.3 meV which would be the value of k_BT for a 485 K thermal beam of OH.

Pioneering studies[36] 25 years ago used laser induced fluorescence (LIF) to measure the internal state distribution of OH radicals at the exit of the corona discharge, OH A $^2\Sigma^+$ → OH X $^2\Pi$. It was found that $T_{rot} = 11$ K and $T_{vib} = 3400 \pm 300$ K. In Note Added in Proof, we estimate the vibrational temperature of the radicals to be 1700−3400 K which implies that between 5% and 22% of the hydroxyl radical beam is $OH_{v=1}$ and the remainder (95% to 78%) is $OH_{v=0}$. Consequently, we believe that all of the hydroxyl radicals impinging on the SAM surface are rotationally ($J'' \leq 5/2$) cold. The translational energy of the beam is 333 cm^{-1} corresponding to a 485 K thermal beam.

In earlier studies,[25,37] the flux of Ar was used to calibrate the EI-QMS. Consequently, we have used this method (see Supporting Information) to calibrate the hydroxyl radical source. As demonstrated in Supporting Information, we believe that the

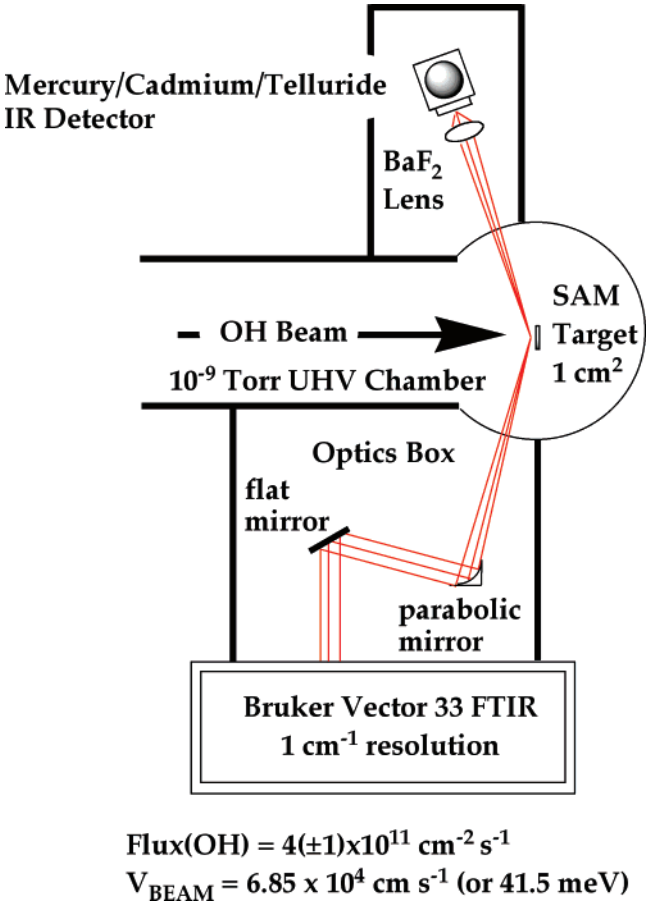

Figure 4. Bruker Vector 33 Fourier transform infrared spectrometer is used to monitor the RAIRS of the SAM surfaces. Roughly 386 scans are collected at 1 cm^{-1} resolution using a properly cleaned polycrystalline Au surface as the background.

corona discharge source in Figures 2 and 3 produces 4 ($\pm$1) $\times$ 10^{11} OH radicals cm^{-2} s^{-1} sharply peaked at 6.85 $\times$ 10^4 cm s^{-1} (41.3 meV).

IR Spectroscopy of SAM Films. The gold surfaces used to make our SAMs were purchased from Platypus Technologies LLC and consist of 1000 Å of polycrystalline Au on cleaned glass slides with a titanium adhesion layer. Monolayers were formed by cleaning the gold surfaces with neat ethanol and drying with nitrogen then exposing the gold surface to roughly a 1 mM solution of the appropriate thiol in ethanol for about 24 h. After adsorption, the surfaces were rinsed thoroughly with ethanol and dried under a stream of nitrogen. In order to study these SAMs, RAIRS is employed as shown in Figure 4.

A Bruker Vector 33 Fourier transform infrared spectrometer is used to characterize our surfaces. Roughly 386 scans are collected at 1 cm^{-1} resolution using a properly cleaned polycrystalline Au surface as the background. A spectrum of the nascent SAM is measured before each oxidation experiment. A globar source is used, and the resulting IR radiation travels through a CaF_2 window and into a turbo-pumped optics box. In the optics box, the collimated IR beam (40 mm) is reflected off of a flat mirror and sent onto a parabolic mirror with an effective focal length of 250 mm. The beam then travels into the surface chamber pumped to 10^{-9} Torr where it reflects off of our SAM target at an incident angle of approximately 77° from the surface normal (grazing angle of 13°). The IR beam exits the surface chamber and passes through a BaF_2 lens (focal length of 38 mm) that focuses it into an external liquid nitrogen cooled broadband mercury cadmium telluride (MCT) detector

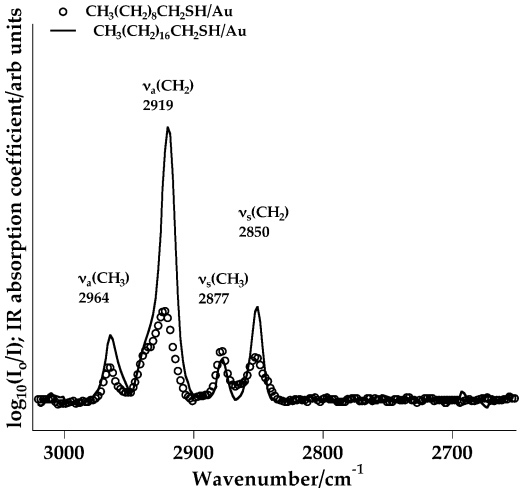

Figure 5. FTIR spectrometer can detect signals from a monolayer of $-CH_3$ groups. This figure displays the spectrum of both decanethiol and octadecanethiol [$CH_3(CH_2)_{17}SH$] SAMs on gold. As expected, the $-CH_2-$ signals grow more intense as the chain length increases.

with a detection area of 1 mm^2. Because of the lenses and windows used, the low-frequency cutoff of our apparatus is around 1000 cm^{-1}. The spectra are taken and processed with OPUS NT 2.06 software.

We have analyzed the RAIRS spectra of the organic SAMs as if the individual chromophores, such as the CH_3- groups, are independent species. However, it is well-known[38] that vibrational modes parallel to ($\nu_{||}$) and near a metal surface are cancelled by image charges while molecular vibrations that are perpendicular to the metallic surface ($\nu_{\perp}$) are enhanced. Consequently, the intensities of the RAIRS spectra will depend not only on the concentration of the IR absorbers but also on their orientation. In fact, the FTIR spectra of alkanethiolate SAMs have been measured successfully.

Alkanethiolate SAMs can be highly uniform films. Polarized RAIRS has been used[39] to deduce the packing and alignment of alkanethiolate SAMs. On polycrystalline Au surfaces, the S···S distance was found to be roughly 5 Å and the alkyl chains are tilted about 26°−28° from the surface normal. Thus, we estimate that the "footprint" for an alkylthiol is roughly 25 $Å^2$ and 1 ML is about 4 $\times$ 10^{14} thiols cm^{-2}. The initial test of the FTIR was to examine the RAIRS spectra of alkane thiol SAMs because the infrared spectra of these films have been so well studied.[39−42] A careful scan of a decanthiol SAM is reported and analyzed in Supporting Information. Figure 5 demonstrates that the FTIR spectrometer can detect signals from a monolayer of $-CH_3$ groups. This figure displays the RAIRS spectrum of both decanethiol and octadecanethiol [$CH_3(CH_2)_{17}SH$] SAMs on gold. As expected, the $-CH_2-$ signals grow more intense as the chain length increases.

Results

1. Reactions of OH Radicals with Alkyl SAMs. When the octadecanethiol SAM was exposed to OH radicals, we observed marked decreases in the CH_3 vibrations within 5 min. The control experiment is presented in Figure S5 (Supporting Information). All of the changes in the IR spectra of the SAMs are induced by OH radicals.

Figure 6 is comprised of five scans that show OH radical reacting with the octadecanethiol film. The initial trace clearly displays the signals in the C−H stretching region: $\nu_a(CH_3)$ at 2964 cm^{-1} and $\nu_s(CH_3)$ at 2878 cm^{-1} as expected from Figure S4 (Supporting Information). Exposure of the film to OH for 1

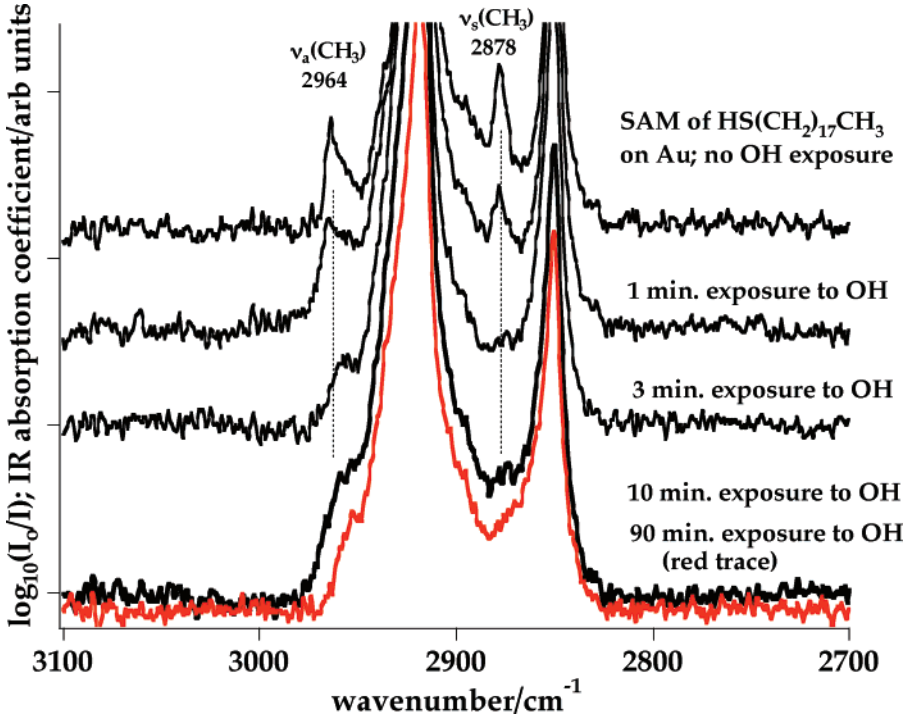

Figure 6. Five scans that show the results of OH radical reacting with the octadecanethiol film. The initial trace clearly displays the signals in the C−H stretching region: $\nu_a(CH_3)$ at 2964 cm^{-1} and $\nu_s(CH_3)$ at 2878 cm^{-1}. Exposure of the film to OH for 1 and 3 min results in degradation of both $\nu_a(CH_3)$ and $\nu_s(CH_3)$ signals; by 10 min both signals are largely destroyed while the CH_2 signals are still intact.

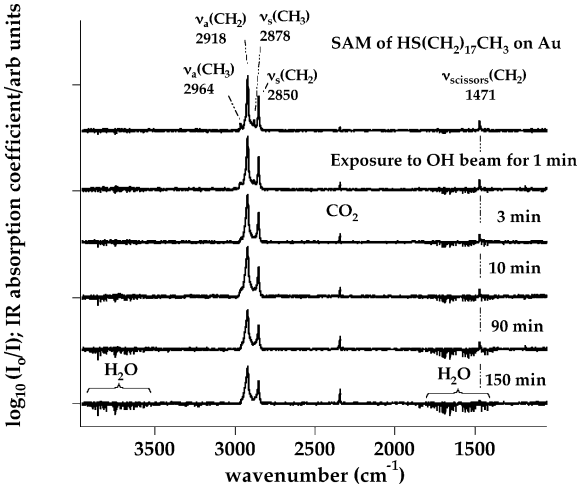

Figure 7. Extended time sequence for OH dosing of an octadecanethiol SAM. After 10 min, reaction at the surface seems to have ceased, and dosing of 2 h has little further effect.

and 3 min results in degradation of both $\nu_a(CH_3)$ and $\nu_s(CH_3)$ signals; by 10 min, both signals are largely destroyed while the CH_2 signals are still intact. Figure 7 is an extended time sequence for OH dosing of an octadecanethiol SAM. After 10 min, reaction at the surface seems to have ceased and dosing of 2 h has little further effect. An exposure time of 10 min to dosing of OH radicals corresponds to (4×10^{11} OH radicals cm^{-2} s^{-1} × 600 s) or impinging of 2.4×10^{14} OH radicals cm^{-2} on the surface. If each hydroxyl radical reacted at the interface, roughly 60% of the terminal $-CH_3$ groups would be destroyed. The feature at 1471 cm^{-1} that is ascribed to a CH_2 scissoring vibration appears to slowly degrade below the noise level in that spectral region after a couple hours. This is most likely to be due to the fact that there is an increased amount of water in the spectra as the experiment proceeds, and therefore, the relatively weak 1471 cm^{-1} absorption becomes more difficult to detect in that region.

All of the evidence suggests that the OH radicals collide with the alkanethiolate SAM and react with the terminal $-CH_3$ groups. Since alkanethiolate/Au SAMs are so regular and closely packed,[22] we believe that the hydroxyl radicals abstract H atoms from the terminal methyl groups to produce alkyl radicals and few of the $-CH_2-$ groups are accessible to the reactive OH radicals. Figure 8 is a sketch of the most likely OH/alkane surface chemistry. The nascent alkyl radicals, $-CH_2\bullet$, are isolated from each other and cannot diffuse on account of the stability of the alkanethiolate/Au SAM. However, as subsequent OH radicals produce more alkyl radicals, they will begin to dimerize and produce a complex set of cross-linked polymers. In the unlikely event that an OH radical would strike a surface-bound radical, radical/radical recombination might occur: $-CH_2\bullet + \bullet OH \rightarrow (-CH_2-OH)^*$. However, the nascent alcohol is unlikely to survive because the chemically activated alcohol, $(-CH_2OH)^*$, must dispose of roughly[19] 95 kcal mol^{-1} of energy. The IR spectrum in Figure 7 shows no evidence of product alcohols.

2. Reactions of OH Radicals with Alkene SAMs. In addition to the reaction of OH with an alkane, we also wanted to study the reaction of hydroxyl radicals with a surface bound alkene. Consequently, we used an undec-10-ene-1-thiol ($HS-(CH_2)_9HC{=}CH_2$)/Au SAM as a target for the OH radical beam. These alkene SAMs have been prepared[43] and used earlier[44] in a study of the heterogeneous oxidation of alkenes by O_3. Hydroxyl radicals react with alkenes by adding[45−48] to the double bond to form a hydroxyalkyl radical.

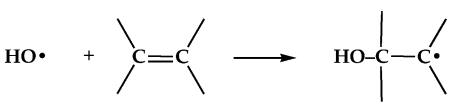

(4)

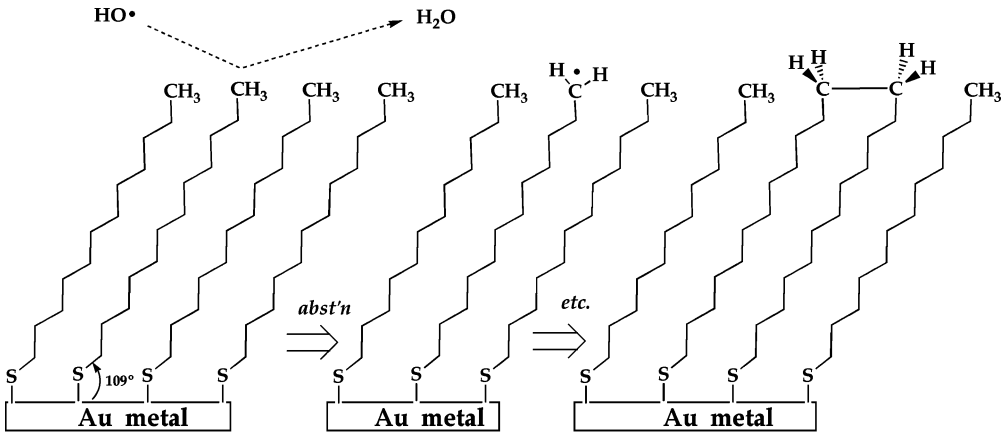

Figure 8. Sketch of the most likely OH/alkane surface chemistry. The nascent alkyl radicals, $-CH_2\bullet$, are isolated from each other and cannot diffuse on account of the stability of the alkanethiolate/Au SAM. Subsequent OH radicals produce more alkyl radicals which begin to dimerize and produce a complex set of cross-linked polymers.

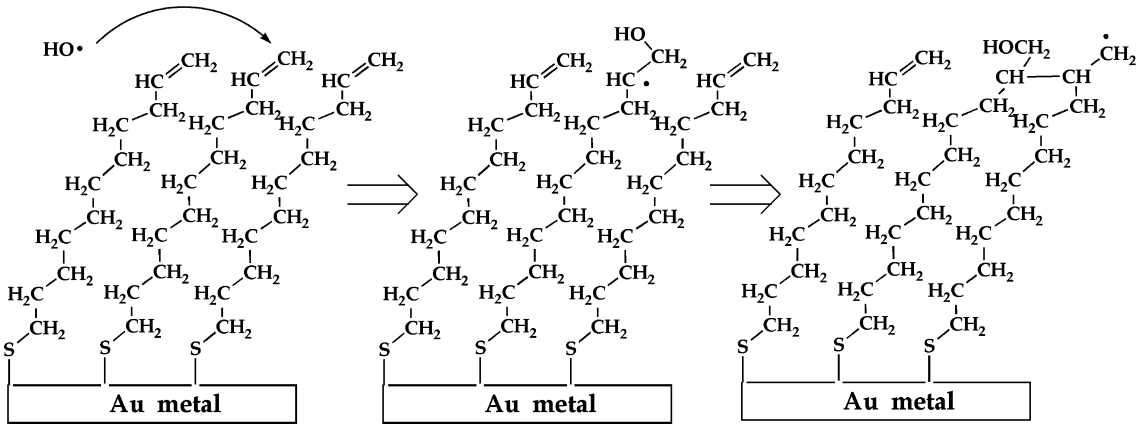

Figure 9. We conjecture that exposure of an alkenthiolate/Au SAM with OH radicals will trigger a radical-induced polymerization resulting in a cross-linked polymeric alcohol.

We expect that exposure of an alkenthiolate/Au SAM with OH radicals will trigger a radical-induced polymerization resulting in a cross-linked polymeric alcohol (see Figure 9). Such a mechanism would lead to a rapid reaction of the monolayer and predicts the selective oxidation of the double bond. However, it will be extremely difficult to detect an alcohol-terminated SAM, as earlier RAIRS spectra[39] of the 16-mercapto-1-hexadecanol SAM, Au/HS$(CH_2)_{15}CH_2OH$, revealed disappointing spectra. There is no hint of the high-frequency O−H stretch (as suggested from the methanol[49] IR spectrum to be roughly 3681 cm^{-1}) while the C−OH stretch is only observed as a weak feature at 1070 cm^{-1} (the corresponding[49] CH_3−OH stretch is $\nu_8 = 1033$ cm^{-1}). Authentic alcohol-terminated SAMs have been studied and do not show the expected OH vibrations because of two reasons. Hydrogen bonding makes this mode extremely broad and difficult to detect, and the surface selection rule states that one is only sensitive to transition dipole moments oriented perpendicular to the surface (the H bonding actually forces the hydroxyl groups to lie parallel to the surface).

The RAIRS spectrum of the HS$(CH_2)_9HC{=}CH_2$/Au SAM is shown in Supporting Information (Figure S6) and is completely assigned. Supporting Information also presents the control experiments (Figure S7) for the HS$(CH_2)_9HC{=}CH_2$/Au SAM. Exposure of the alkene film to a beam of OH with the corona discharge off and the hexapole filter on has no effect on the SAM. Likewise, dosing the film with the beam resulting from an active corona discharge but with the hexapole filter off only induces minor changes in the film.

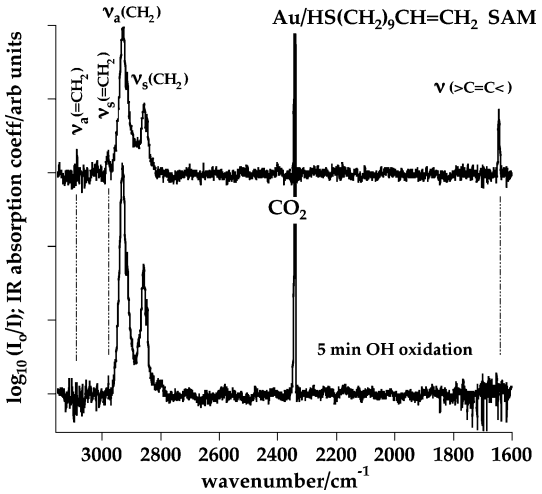

Figure 10. IR spectrum of undec-10-ene-1-thiol on gold before and after oxidation with OH radicals. The top trace is the SAM before oxidation and the bottom scan is the SAM after 5 min of oxidation, respectively. These spectra demonstrate that the double bond is selectively oxidized by the OH radical while the alkyl chain of the SAM remains intact.

Figure 10 illustrates the IR spectrum of undec-10-ene-1-thiol on gold before and after oxidation with OH radicals. The top trace is the SAM before oxidation and the bottom scan is the SAM after 5 min of oxidation, respectively. These spectra demonstrate that the double bond is selectively oxidized by the

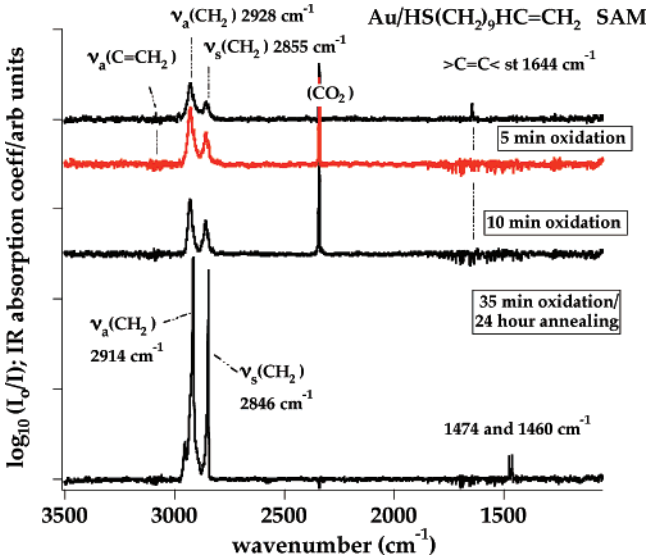

Figure 11. Results from longer exposure times of the HS(CH$_2$)$_9$HC=CH$_2$/Au SAM with OH radicals. The alkene SAM was dosed for 35 min with hydroxyl radicals and left overnight. Following a 24 h annealing in the UHV chamber, the CH_2 stretches become sharpened and red-shifted by 10 cm^{-1}. We believe that the SAM surface is polymerizing and becoming more uniform with time.

OH radical while the alkyl chain of the SAM remains intact. After 5 min of OH dosing, the >C=C< bond is largely destroyed because ν(>C=C<) is no longer detected. During this time, the surface has been exposed to 10^{14} hydroxyl radicals (corresponding to collisions with roughly 30% of the molecules in the SAM), and all IR signals associated with the terminal alkene, [ν(>C=C<), ν_a(=CH$_2$), ν_s(=CH$_2$)], have vanished.

Results from longer exposure times of the HS(CH$_2$)$_9$HC=CH$_2$/Au SAM with OH radicals are shown in Figure 11. In this experiment, the alkene SAM was dosed for 35 min with hydroxyl radicals and left overnight. Following a 24 h annealing in the UHV chamber, the CH_2 stretches become sharpened and red-shifted (by about 10 cm^{-1}). This may suggest that the SAM surface is polymerizing and becoming more uniform with time. In addition, two new peaks grow in at 1474 cm^{-1} and 1460 cm^{-1}, which are in the region of CH_2 bending modes.

Discussion

We have studied the oxidation of self-assembled monolayers of alkanes and alkenes with a thermal beam of OH radicals. The target films were produced by bonding alkane thiols and alkene thiols to a gold surface, and the SAMs were mounted in a vacuum chamber at a base pressure of 10^{-9} Torr. Hydroxyl radicals were produced by a corona discharge of a H_2O_2/water mixture. The resultant molecular beam is filtered by an electrostatic hexapole, and the OH radicals are selectively focused onto the target SAM. We are able to produce beams of OH radicals with a flux of 4 ($\pm$1) $\times$ 10^{11} OH radicals cm^{-2} sec^{-1}.

The infrared spectra presented in this paper clearly show that OH radicals are reacting with hydrocarbon SAMs mounted on gold surfaces. For alkane surfactants, the RAIRS demonstrates that dosing of an octadecane thiol SAM with OH radicals largely destroys the CH_3- groups at the surface in 10 min. Octadecane is an alkane, and the OH radical can only abstract a H atom to produce an alkyl radical; $\bullet OH + CH_3- \rightarrow H_2O + \bullet CH_2-$. Since the flux (OH) in our experiments is 4 ($\pm$1) $\times$ 10^{11} radicals cm^{-2} s^{-1}, during the 10 min dosing time, about 60% of a ML for the SAM could be oxidized if the OH reaction probability is 100%. The fate of the resulting interfacial alkyl radicals, $\bullet CH_2-$, could not be determined by RAIRS. In contrast to alkanes, we believe that hydroxyl radicals add to the double bonds of alkenes;

$$\bullet OH + >C=C< \rightarrow HO-\overset{|}{C}-\overset{|}{\dot{C}}<.$$

Oxidation of the undec-10-ene-1-thiol (HS(CH$_2$)$_9$HC=CH$_2$) SAM with the calibrated OH radical source consumes the terminal alkene, CH_2=CH$-$, within 5 min. Application of 1 $\times$ 10^{14} hydroxyl radicals cm^{-2}, roughly $^1/_4$ ML of the alkene, triggers the disappearance of the interfacial double bonds. This is faster than H atom abstraction and might be an indication that the OH radicals are triggering free radial polymerization of the unsaturated SAM.

Figures 7 and 11 demonstrate that prolonged exposure to OH radicals does not completely degrade the aliphatic carbon chains. The RAIRS spectra in Figure 7 demonstrate that large parts of the octadecane thiol SAM remain intact and stable after 150 min of dosing with OH (corresponding to the number of OH radicals cm^{-2} being 9 times the number of molecules cm^{-2} in the ML). Figure 11 follows the evolution of undec-10-ene-1-thiol SAM for 35 min of OH dosing during which time these alkenes are exposed to 2 ML of hydroxyl radicals. The RAIRS spectra in Figures 7 and 11 demonstrate that there is an initial period of 5$-$10 min during which the hydrocarbons are oxidized. After these first reactions, further dosing of the SAMs with OH radicals does not seem to affect them.

The behavior of the $-CH_2-$ modes after the "24 h" anneal (Figure 11) is remarkable. There is a dramatic intensity increase after a reaction that is accompanied by an extremely large red-shift in energy. We suspect that there is a major structural change in the SAM that is not likely to be simply ordering. Actually, the surface selection rule makes the intensity of the $-CH_2-$ stretches lower than they should otherwise be. In a "normal" SAM, the ordering makes a significant component of the transition dipole moment lie parallel to the surface thus diminishing the RAIRS signal. This is why disordering increases the intensity. However, the features in the annealed spectrum of Figure 11 are much too narrow for a disordered surface. The width of the features at 2914 cm^{-1} and 2846 cm^{-1} is actually a better indicator of order than the frequency shift. We speculate that a polymerization reaction has been triggered by the OH radicals and that the resulting polymer has a dramatically different structure than the original SAM.

The long-term stability of alkyl SAMs that are exposed to OH beams in high vacuum (10^{-9} Torr in Figure 2) can be contrasted with the results of Molina et al.[50] who studied the evolution of organic films mounted in a flow tube. Thin films (2.5 nm) of octadecyltrichlorosilane (OTS) were deposited on glass slides and exposed to a stream of OH radicals ($\cong 10^8$ cm^{-3}) entrained in a flow of 1 Torr O_2, 0.1 mTorr NO and NO_2, and 20 mTorr H_2O. Complementary studies with infrared spectroscopy, X-ray photoelectron spectroscopy, and atomic force microscopy reveal that the entire hydrocarbon film is destroyed within 15 min. In 1999, it was predicted that oxidation of organic aerosols would produce a large number of oxygenated volatile organic compounds (OVOC) in the remote troposphere.[9] The rapid destruction of OTS films is consistent with this prediction.[50] Recent atmospheric field studies[51] continue to support the notion of organic aerosols as a source of OVOCs.

These rapid flow tube oxidations[50] are likely to be the result of many radical chain mechanisms. Exposure of an OTS film with 10^8 hydroxyls cm^{-3} for 15 min corresponds to exposure of roughly 1 ML OH radicals. The nascent alkyl radicals that

are produced by OH are certainly intercepted by the O_2, NO, and NO_2 in the flow tube, and a complex set of surface oxidations must ensue. The experiments in the current paper are only concerned with the initial OH radical reactions. There is clearly a huge amount of work to be done to unravel these complex chemical pathways.

Note Added in Proof. We have carefully considered the possibility that the radical source might produce vibrationally excited OH radicals. Almost 25 years ago,[36] LIF spectra of hydroxyl radicals produced by a corona discharge suggested a vibrational temperature of T_{vib}(OH) to be 3400 ± 300 K. In separate experiments, the hydroxyl radicals that were generated with an electrical discharge were detected by (2 + 1) resonance-enhanced ionization spectroscopy [Greenslade, M. E.; Lester, M. I.; Radenovic, D. C.; van Roij, A. J. A.; Parker, D. H. *J. Chem. Phys.* **2005**, *123*, 074309], and it was determined that T_{vib} was 1700 K. The vibrational lifetime of hydroxyl radicals has been directly measured in the last two years. A pulsed beam of vibrationally excited OH radicals was Stark decelerated and loaded into an electrostatic quadrupole trap [van de Meerakker, S. Y. T.; Vanhaecke, N.; van der Loo, M. P. J.; Groenenboom, G. C.; Meijer, G. *Phys. Rev. Lett.* **2005**, *95*, 013003]. The radiative lifetime of the upper Λ-doublet component of the OH $X\ ^2\Pi_{3/2}v = 1$ level was determined as 59.0 ± 2.0 ms. Consequently, to be conservative, we estimate that the vibrational temperature of the hydroxyl radicals produced by the source in Figures 2 and 3 is somewhere between 1700 and 3400 K. The OH radicals suffer no collisions during the 2 ms flight time from the corona discharge to the SAM target (see Figures 2 and 3). A vibrational temperature between 1700 and 3400 K implies that between 5% and 22% of the hydroxyl radical beam is $OH_{v=1}$ and the raminder (95% to 78%) is $OH_{v=0}$ $[n[(v = 1)/n(v = 0) = \exp(-3566\ cm^{-1}/k_BT_{vib}]$.

Acknowledgment. The experimental apparatus in Figures 2 and 3 was designed and fabricated by the Integrated Instrument Design Facility at CIRES in the University of Colorado. We would like to thank our instrument makers for a superb job on the design and fabrication of this unique radical/surface instrument. We would like to thank Prof. Bruce E. Koel for several helpful discussions. This work was supported by grants from the Condensed Phase Interfacial Molecular Science Program, United States Department of Energy (DE-DF02-93ER14364) and the National Science Foundation (CHE-9813659) to G.B.E.

Supporting Information Available: Calibration of the OH source, plot of J_{Ar} for different source pressures vs I^+, extent of the Stark focusing of OH radicals as the voltage is varied, FTIR spectrum, control experiment for dosing of OH radicals with alkane SAM, RAIRS spectrum, control experiment for the OH oxidation of $HS(CH_2)_9HC{=}CH_2$/Au SAM. This material is available free of charge via the Internet at http://pubs.acs.org.

References and Notes

(1) Atkinson, R.; Arey, J. *Chem. Rev.* **2003**, *103*, 4605.

(2) Atkinson, R. *Atmos. Chem. Phys.* **2003**, *3*, 2233.

(3) Heard, D. E.; Pilling, M. J. *Chem. Rev.* **2003**, *103*, 5163.

(4) Smith, S. C.; Lee, J. D.; Bloss, W. J.; Johnson, G. P.; Ingham, T.; Heard, D. E. *Atmos. Chem. Phys.* **2006**, *6*, 1435.

(5) Heard, D. E. *Annu. Rev. Phys. Chem.* **2006**, *57*, 191.

(6) Wennberg, P. O. *Nature* **2006**, *442*, 145.

(7) Rohrer, F.; Berresheim, H. *Nature* **2006**, *442*, 184.

(8) Pruppacher, H. R.; Klett, J. D. *Microphysics of Clouds and Precipitation*, 2nd ed.; Kluwer Academic Publishing: Dordrecht, Holland, 1997.

(9) Ellison, G. B.; Tuck, A. F.; Vaida, V. *J. Geophys. Res.-Atmos.* **1999**, *104*, 11633.

(10) Seinfeld, J. H.; Pandis, S. N. *Atmospheric Chemistry and Physics: From Air Pollution to Climate Change*; John Wiley & Sons: New York City, 1998.

(11) Rudich, Y.; Benjamin, I.; Naaman, R.; Thomas, E.; Trakhtenberg, S.; Ussyshkin, R. *J. Phys. Chem. A* **2000**, *104*, 5238.

(12) Tervahattu, H.; Hartonen, K.; Kerminen, V. M.; Kupiainen, K.; Aarnio, P.; Koskentalo, T.; Tuck, A. F.; Vaida, V. *J. Geophy. Res.-Atmos.* **2002**, *107*.

(13) Wyslouzil, B. E.; Wilemski, G.; Strey, R.; Heath, C. H.; Dieregsweiler, U. *Phys. Chem. Chem. Phys.* **2006**, *8*, 54.

(14) Anttila, T.; Kiendler-Scharr, A.; Mentel, T. F.; Tillmann, R. *J. Atmos. Chem.* **2007**, *57*, 215.

(15) Nilsson, E. D.; Mårtensson, E. M.; Van Ekeren, J. S.; de Leeuw, G.; Moerman, M.; O'Dowd, C. *Atmos. Chem. Phys. Discuss.* **2007**, *7*, 13345.

(16) Ruscic, B.; Feller, D.; Dixon, D. A.; Peterson, K. A.; Harding, L. B.; Asher, R. L.; Wagner, A. F. *J. Phys. Chem. A* **2001**, *105*, 1.

(17) Ruscic, B.; Boggs, J. E.; Burcat, A.; Csaszar, A. G.; Demaison, J.; Janoschek, R.; Martin, J. M. L.; Morton, M. L.; Rossi, M. J.; Stanton, J. F.; Szalay, P. G.; Westmoreland, P. R.; Zabel, F.; Berces, T. *J. Phys. Chem. Ref. Data* **2005**, *34*, 573.

(18) Berkowitz, J.; Ellison, G. B.; Gutman, D. *J. Phys. Chem.* **1994**, *98*, 2744.

(19) Blanksby, S. J.; Ellison, G. B. *Acc. Chem. Res.* **2003**, *36*, 255.

(20) Donahue, N. M.; Anderson, J. G.; Demerjian, K. L. *J. Phys. Chem. A* **1998**, *102*, 3121.

(21) Bertram, A. K.; Ivanov, A. V.; Hunter, M.; Molina, L. T.; Molina, M. J. *J. Phys. Chem. A* **2001**, *105*, 9415.

(22) Ulman, A. *Chem. Rev.* **1996**, *96*, 1533.

(23) Zorn, J. C.; English, T. C. *Adv. Atomic Mol. Phys.* **1973**, *9*, 243.

(24) Hain, T. D.; Weibel, M. A.; Backstrand, K. M.; Pope, P. E.; Curtiss, T. J. *Chem. Phys. Lett.* **1996**, *262*, 723.

(25) Hain, T. D.; Weibel, M. A.; Backstrand, K. M.; Curtiss, T. J. *J. Phys. Chem. A* **1997**, *101*, 7674.

(26) Bernstein, R. B. *Chemical Dynamics via Molecular Beam and Laser Techniques*; Oxford University Press: Oxford, 1982.

(27) Peterson, K. I.; Fraser, G. T.; Klemperer, W. *Can. J. Phys.* **1984**, *62*, 1502.

(28) Nelson, D. D.; Schiffman, A.; Nesbitt, D. J.; Orlando, J. J.; Burkholder, J. B. *J. Chem. Phys.* **1990**, *93*, 7003.

(29) Hain, T. D.; Baars-Hibbe, L.; Curtiss, T. J. *Chem. Phys. Lett.* **1999**, *305*, 348.

(30) Hain, T. D.; Moision, R. M.; Curtiss, T. J. *J. Chem. Phys.* **1999**, *111*, 6797.

(31) Engelking, P. C. *Rev. Sci. Instrum.* **1986**, *57*, 2274.

(32) Engelking, P. C. *Chem. Rev.* **1991**, *91*, 399.

(33) Tarnovsky, V.; Deutsch, H.; Becker, K. *J. Chem. Phys.* **1998**, *109*, 932.

(34) Lindeman, L. P.; Guffy, J. C. *J. Chem. Phys.* **1958**, *29*, 247.

(35) Miller, D. R. Free Jet Sources. In *Atomic and Molecular Beam Methods*; Scoles, G., Bassi, D., Buck, U., Lainé, D., Eds.; Oxford University Press: New York, 1988; Vol. 1, p 14.

(36) Droege, A. T.; Engelking, P. C. *Chem. Phys. Lett.* **1983**, *96*, 316.

(37) Bickes, R. W.; Newton, K. R.; Herrmann, J. M.; Bernstein, R. B. *J. Chem. Phys.* **1976**, *64*, 3648.

(38) Ulman, A. *An Introduction to Ultrathin Organic Films*; Academic Press: San Diego, 1991.

(39) Nuzzo, R. G.; Dubois, L. H.; Allara, D. L. *J. Am. Chem. Soc.* **1990**, *112*, 558.

(40) Macphail, R. A.; Snyder, R. G.; Strauss, H. L. *J. Chem. Phys.* **1982**, *77*, 1118.

(41) Macphail, R. A.; Strauss, H. L.; Snyder, R. G.; Elliger, C. A. *J. Phys. Chem.* **1984**, *88*, 334.

(42) Nuzzo, R. G.; Korenic, E. M.; Dubois, L. H. *J. Chem. Phys.* **1990**, *93*, 767.

(43) Peanasky, J. S.; McCarley, R. L. *Langmuir* **1998**, *14*, 113.

(44) Fiegland, L. R.; Saint Fleur, M. M.; Morris, J. R. *Langmuir* **2005**, *21*, 2660.

(45) Jenkin, M. E.; Saunders, S. M.; Pilling, M. J. *Atmos. Environ.* **1997**, *31*, 81.

(46) Jenkin, M. E.; Saunders, S. M.; Wagner, V.; Pilling, M. J. *Atmos. Chem. Phys.* **2003**, *3*, 181.

(47) Saunders, S. M.; Jenkin, M. E.; Derwent, R. G.; Pilling, M. J. *Atmos. Chem. Phys.* **2003**, *3*, 161.

(48) DeMore, W. B.; Sander, S. P.; Golden, D. M.; Molina, M. J.; Hampson, R. F.; Kurylo, M. J.; Howard, C. J.; Ravishankara, A. R.; Kolb, C. E.; Molina, M. J. *Chemical Kinetics and Photochemical Data for Use in Stratospheric Modeling: Evaluation Number 12*; NASA, 1997.

(49) Shimanouchi, T. *Tables of Molecular Vibrational Frequencies, Consolidated Vol. I*; National Bureau of Standards: Washington, D. C., 1972; Vol. I (NSRDS-NBS 39).

(50) Molina, M. J.; Ivanov, A. V.; Trakhtenberg, S.; Molina, L. T. *Geophys. Res. Lett.* **2004**, *31*.

(51) Kwan, A. J.; Crounse, J. D.; Clarke, A. D.; Shinozuka, Y.; Anderson, B. E.; Crawford, J. H.; Avery, M. A.; McNaughton, C. S.; Brune, W. H.; Singh, H. B.; Wennberg, P. O. *Geophys. Res. Lett.* **2006**, *33*.